

Real-Time Flux-weakening Control for an IPMSM Drive System Using a Predictive Controller

Tian-Hua Liu*, Shao-Kai Tseng, Yi Chen, Mao-Bin Lu

Department of Electrical Engineering, National Taiwan University of Science and Technology, 106, Taiwan

ARTICLE INFO

Received: 07 October, 2017

Accepted: 29 October, 2017

Online: 10 November, 2017

Keywords :

predictive controller

real-time tuning

flux-weakening control

IPMSM

ABSTRACT

This paper proposes extended-range high-speed control for an IPMSM drive system. A simple real-time tuning flux-weakening control algorithm is proposed and implemented to control an IPMSM drive system in a wide variable speed range, from 3 r/min up to 2700 r/min. This flux-weakening control algorithm does not require any motor parameters and only needs simple mathematical computations. The proposed drive system adjusts the angle between the d-axis and q-axis current to reach flux-weakening control. In addition, a multiple sampling predictive controller is implemented to enhance the dynamic responses of the proposed drive system, which yields improved overall transient responses, superior load responses, and good tracking responses. A detailed analysis of the proposed drive system's stability is discussed as well. A 32-bit digital signal processor, TMS-320F-28335, is used to execute the predictive controller and the flux-weakening control algorithm for the IPMSM drive system. Experimental results can validate the theoretical analysis.

1. Introduction

Use of the interior permanent magnet synchronous motor (IPMSM) has greatly increased due to its advantages over other motors, which include high efficiency, wide operating speed range, high power density, and robustness. The IPMSM has two different torque components: electromagnetic torque and reluctance torque. By strategically controlling the d-axis and q-axis currents, the maximum torque per ampere (MTPA) control or flux weakening control can be achieved at different operating speeds.

This paper is an extension of work originally presented in 2017 IEEE 26th International Symposium on Industrial Electronics (ISIE) Conference [1]. Several researchers have proposed different flux-weakening control methods to increase the high-speed operating range of an IPMSM. For example, Bolognani et al. proposed an adaptive flux-weakening controller for an IPMSM drive system. The adaptation algorithm, however, is very complicated to implement [2]. Zhu et al. implemented a flux-weakening control for a PMSM drive system [3]. The proposed method accounted for resistance voltage drop and inverter nonlinearities. This method, however, is only suitable for a PMSM drive system, not an IPMSM drive system. Kwon et al. proposed a flux-weakening control for an IPMSM with quasi-six-step operation [4]. A feed-forward path, which consists of a one

dimensional look-up table, is required. Pan et al. proposed a robust flux-weakening control strategy for a surface-mounted permanent-magnet motor drive [5]. A closed-form solution of the maximum available torque-producing current is generated to achieve both fast responses and real-time tuning flux-weakening control. This method, however, is suitable for a surface mounted PMSM but not an IPMSM. Uddin et al. proposed an on-line parameter-estimation-based high-speed control of an IPMSM drive. The method of estimating the d-axis inductance, q-axis inductance, and external load, however, is very complicated [6]. Pan et al. proposed a voltage-constraint-based flux-weakening control of an IPMSM drive system [7]. The method requires a d-axis current command and q-axis current command generator, which is rather complicated. Jung et al. proposed a hexagonal voltage limit to increase the voltage amplitude and to improve the DC-link voltage utilization in an IPMSM drive system. A torque control method based on the voltage angle was investigated. The idea is very good; however, the voltage vector selection algorithm is very complicated [8]. Chaithongsuk et al. proposed an optimal design of permanent magnet motors to improve flux-weakening performance in variable speed drives. It was shown that a salient-pole motor performed better at high speeds than a non-salient pole motor [9]. Kim proposed a novel magnetic flux-weakening method for permanent magnet synchronous motors in electric vehicles [10]. By adjusting the air gap between the stator and rotor, an increased maximum speed and maximum output power could be

*Corresponding Author: Tian-Hua Liu, Mobile: +886-22737-6108

Email: Liu@mail.ntust.edu.tw

www.astesj.com

<https://dx.doi.org/10.25046/aj060210>

obtained. This method, however, requires very complicated motor modifications. Jevremovic et al. proposed a simple robust integral controller to achieve field weakening control for a PMSM [11]. Harnefors et al. used a systematic analysis to determine the parameters of the current and speed combined controller to reduce the complicity [12]. To improve the performance of field weakening control, Wallmark et al. [13] and Bedetti et al. implemented a voltage regulator to achieve flux-weakening control for an electric vehicle and an IPMSM [14].

In this paper, a simple flux-weakening control method is proposed. This method has several advantages over previously proposed flux-weakening methods [1]-[14]. For one thing, the parameters of the IPMSM are not required. Also, the computations for the flux-weakening control are very simple. For example, only square root, multiplication, and addition are used. In addition, to achieve fast responses and good load disturbance rejection capability from the low-speed range to high-speed range, a predictive controller is employed. In contrast to previous research on predictive control [15]-[16], this paper proposes a multiple-loop predictive control motor drive system. The sampling interval of the current-loop is 100, and the sampling interval of the speed-loop is 1 ms. Due to the quick current regulation, the proposed system has better performance than previous one-loop predictive control drive systems [15]-[16]. Unlike previous methods of flux-weakening control without using motor parameters [2], [16]-[17], the proposed method provides a simple control algorithm for voltage regulation without an adaptive controller or PI controller. To the authors' best knowledge, the proposed flux-weakening control method is a new idea. In addition, the idea of the predictive controller applied in the simplified flux-weakening control of an IPMSM is original.

2. Predictive Controller Design

The theory of predictive control was first proposed in the 1970s, and predictive controllers have been used in chemical and steel processing for more than 40 years. Recently, predictive control has been applied in motor drives due to the fast computation ability of the digital signal processor (DSP). The design objective of a predictive controller is to compute the control input u to optimize the future dynamic behavior for the output y of the plant. This optimization must be performed within a limited time window. Several researchers have investigated predictive control for motor drives. For example, Pacas et al. proposed a predictive direct torque control for PMSMs, which yielded a faster torque settling time than the classic field-oriented control with a PI controller [15]. Bolognani et al. investigated the design and implementation of model predictive control for electric motor drives [16]. Fuentes et al. implemented a predictive speed control for a two-mass system driven by a PMSM. Their proposed method allowed feedback of all the mechanical and electrical state variables into a single control input and provided a higher bandwidth closed-loop speed control [18]. Siami et al. proposed an improved predictive current control using prediction error correction for PMSMs [19]. Tarczewski et al. implemented a constrained state feedback speed control for PMSMs, which calculated the boundaries of control signals to provide permissible values of the future state variables [20].

In this paper, a systematic predictive controller design is proposed for an IPMSM drive system. The proposed predictive controllers, including a predictive current controller and a predictive speed controller, provide a multiple sampling rate control system and a closed-loop speed-control block diagram that are different from the predictive controllers proposed in previously published papers [15]-[16], [18]-[20].

The design of a predictive controller requires the following. First, a model of the uncontrolled drive system is developed. Next, a cost function that represents the desired behavior of the system is defined. Finally, a predictive controller for the motor drive system is derived.

2.1. Predictive Current Controller

The state-variable equation of an IPMSM can be expressed as

$$\frac{d}{dt} \begin{bmatrix} i_d \\ i_q \end{bmatrix} = \begin{bmatrix} -\frac{r_s}{L_d} & 0 \\ 0 & -\frac{r_s}{L_q} \end{bmatrix} \begin{bmatrix} i_d \\ i_q \end{bmatrix} + \begin{bmatrix} \frac{1}{L_d} & 0 \\ 0 & \frac{1}{L_q} \end{bmatrix} \begin{bmatrix} v_d \\ v_q \end{bmatrix} + \begin{bmatrix} \frac{1}{L_d} & 0 \\ 0 & \frac{1}{L_q} \end{bmatrix} \begin{bmatrix} \omega_{re} L_q i_q \\ -\omega_{re} (L_d i_d + \lambda_m) \end{bmatrix} \quad (1)$$

Where d/dt is the differential operator, i_d and i_q are the d-axis and q-axis stator currents, r_s is the stator resistance, v_d and v_q are the d-axis and q-axis stator voltages, L_d and L_q are the d-axis and q-axis self-inductances, λ_m is the permanent magnetic flux leakage, and ω_{re} is the electric motor speed.

After transferring the continuous-time domain into the discrete-time domain, (1) can be expressed as

$$i_d(z) = \frac{\beta_{cd} z^{-1}}{1 - \alpha_{cd} z^{-1}} (v_d - \omega_{re} L_q i_q) \quad (2)$$

and

$$i_q(z) = \frac{\beta_{cq} z^{-1}}{1 - \alpha_{cq} z^{-1}} (v_q - \omega_{re} (L_d i_d + \lambda_m)) \quad (3)$$

The related parameters in (2) and (3) are shown as follows

$$\alpha_{cd} = e^{-\frac{r_s T_{cur}}{L_d}} \quad (4a)$$

$$\beta_{cd} = \frac{1}{r_s} (1 - \alpha_{cd}) \quad (4b)$$

$$\alpha_{cq} = e^{-\frac{r_s T_{cur}}{L_q}} \quad (4c)$$

$$\beta_{cq} = \frac{1}{r_s} (1 - \alpha_{cq}) \quad (4d)$$

where T_{cur} is the sampling interval of current-loop control. Because the sampling time interval is shorter than the time constant of the stator current-loop, Euler approximation can be used here. As a result, the parameters shown in (4a)-(4d) can be described as follows

$$\alpha_{cd} \approx 1 - \frac{r_s T_{cur}}{L_d} \quad (5a)$$

$$\beta_{cd} \approx \frac{r_s T_{cur}}{L_d} \quad (5b)$$

$$\alpha_{cq} \approx 1 - \frac{r_s T_{cur}}{L_q} \quad (5c)$$

and

$$\beta_{cq} \approx \frac{r_s T_{cur}}{L_q} \quad (5d)$$

Then (2) and (3) can be rewritten as follows

$$X_{cur}(k+1) = A_{cur} X_{cur}(k) + B_{cur} U_{cur}(k) + B_{cur} F_{cur}(k) \quad (6)$$

and

$$X_{cur}(k) = [i_d(k) \quad i_q(k)]^T \quad (7a)$$

$$F_{cur}(k) = [\omega_{re}(k)L_q i_q(k) \quad -\omega_{re}(k)(L_d i_d(k) + \lambda_m)]^T \quad (7b)$$

$$U_{cur}(k) = [v_d(k) \quad v_q(k)]^T \quad (7c)$$

$$A_{cur} = \begin{bmatrix} 1 - \frac{r_s T_{cur}}{L_d} & 0 \\ 0 & 1 - \frac{r_s T_{cur}}{L_q} \end{bmatrix} \quad (7d)$$

$$B_{cur} = \begin{bmatrix} \frac{T_{cur}}{L_d} & 0 \\ 0 & \frac{T_{cur}}{L_q} \end{bmatrix} \quad (7e)$$

According to (6), the (k+1)-th predictive current can be expressed as

$$\hat{X}_{cur}(k+1) = A_{cur} X_{cur}(k) + B_{cur} (U_{cur}(k) + F_{cur}(k)) \quad (8)$$

The performance index of the d-axis current control is defined as

$$J_{cur} = [\hat{i}_d(k+1) - i_d^*(k+1)]^2 \quad (9)$$

The following equation is the partial differential of (9) manipulated to equal zero.

$$\frac{\partial J_{cur-d}}{\partial U_d} = \frac{\partial (\hat{i}_d(k+1) - i_d^*(k+1))^2}{\partial v_d(k)} = 0 \quad (10)$$

Substituting (8) into (10), we can obtain

$$\begin{aligned} \frac{\partial J_{cur-d}}{\partial v_d(k)} &= \frac{\partial \left(\left(1 - \frac{T_{cur} r_s}{L_d}\right) i_d(k) + \left(\frac{T_{cur}}{L_d}\right) (v_d(k) + \omega_{re}(k)L_q i_q(k)) - i_d^*(k+1) \right)^2}{\partial v_d(k)} \\ &= 2 \left(\left(1 - \frac{T_{cur} r_s}{L_d}\right) i_d(k) + \left(\frac{T_{cur}}{L_d}\right) (v_d(k) + \omega_{re}(k)L_q i_q(k)) - i_d^*(k+1) \right) \left(\frac{T_{cur}}{L_d}\right) = 0 \end{aligned} \quad (11)$$

After arranging the above, it is not difficult to obtain

$$\begin{aligned} &\left(\left(1 - \frac{T_{cur} r_s}{L_d}\right) i_d(k) + \left(\frac{T_{cur}}{L_d}\right) (v_d(k) + \omega_{re}(k)L_q i_q(k)) - i_d^*(k+1) \right) \\ &= \left(\left(\frac{L_d}{T_{cur}} - r_s\right) i_d(k) + (v_d(k) + \omega_{re}(k)L_q i_q(k)) - \frac{L_d}{T_{cur}} i_d^*(k+1) \right) = 0 \end{aligned} \quad (12)$$

Finally, from (12), we can derive the d-axis voltage command as

$$v_d^*(k) = r_s i_d(k) + \frac{L_d}{T_{cur}} (i_d^*(k+1) - i_d(k)) - \omega_{re}(k)L_q i_q(k) \quad (13)$$

By using the same principle, we can derive the q-axis voltage command as follows

$$v_q^*(k) = r_s i_q(k) + \frac{L_q}{T_{cur}} (i_q^*(k+1) - i_q(k)) + \omega_{re}(k)(L_d i_d(k) + \lambda_m) \quad (14)$$

2.2. Predictive Speed Controller

The differential equation of an IPMSM is

$$\frac{d}{dt} \omega_{rm} = \frac{1}{J_m} (T_e - T_L - B_m \omega_{rm}) \quad (15)$$

Where J_m is the mechanical inertia, ω_{rm} is the mechanical speed, $\frac{d}{dt}$ is the differential operator, T_e is the total output torque, T_L is the external load, and B_m is the viscous frictional coefficient.

According to (15) and assuming $T_L = 0$, the speed can be expressed as

$$\omega_{rm}(s) = \frac{T_e}{J_m s + B_m} \quad (16)$$

By converting (16) into discrete form, one can obtain

$$\begin{aligned} \omega_{rm}(k+1) &= e^{-(B_m/J_m)T_{sp}} \omega_{rm}(k) + \frac{1}{B_m} (1 - e^{-(B_m/J_m)T_{sp}}) T_e(k) \\ &= a_1 \omega_{rm}(k) + b_1 u(k) \end{aligned} \quad (17)$$

and

$$a_1 = e^{-(B_m/J_m)T_{sp}} \quad (18)$$

$$b_1 = \frac{1}{B_m} (1 - e^{-(B_m/J_m)T_{sp}}) \quad (19)$$

$$u(k) = T_e(k) \quad (20)$$

where T_{sp} is the sampling interval of the speed-loop control. Next, by setting the predictive window as 1 and the predictive control as 1, the performance index J_{sp} is expressed as

$$\begin{aligned} J_{sp} &= \sum_{i=1}^1 [P(z) \hat{\omega}_{rm}^{pre}(k+i) - P(1) \omega_{rm}^*(k+i)]^2 \\ &\quad + \rho \sum_{i=1}^1 [Q(z) u(k+i-1)]^2 \end{aligned} \quad (21)$$

where $\hat{\omega}_{rm}^{pre}$ is the predictive speed, $P(z)$ and $Q(z)$ are polynomials of Z , and ρ is the weighting factor. By computing

$\frac{\partial J_{sp}}{\partial u(k)}$, one can obtain

$$\begin{aligned} \frac{\partial J_{sp}}{\partial u(k)} &= 2 \frac{P(z) \partial \hat{\omega}_{rm}^{pre}(k+1)}{\partial u(k)} [P(z) \hat{\omega}_{rm}^{pre}(k+1) \\ &\quad - P(1) \omega_{rm}^*(k+1)] + 2\rho Q^2(z) u(k) = 0 \end{aligned} \quad (22)$$

Substituting (17) into (22), one can derive

$$\begin{aligned} P(z) b_1 (P(z) (b_1 u(k) + a_1 \omega_{rm}(k)) - P(1) \omega_{rm}^*(k+1)) \\ + \rho Q^2(z) u(k) = 0 \end{aligned} \quad (23)$$

The speed command at (k+1)th sampling interval can be expressed as a fixed command S_p and then can be defined as

$$\omega_{rm}^*(k+1) = S_p \quad (24)$$

By substituting (24) into (23), we can obtain

$$(P(z) b_1)^2 u(k) + \rho Q^2(z) u(k) = P(z) b_1 P(1) S_p - P^2(z) b_1 a_1 \omega_{rm}(k) \quad (25)$$

The control input can be expressed as

$$u(k) = R(M S_p - N \omega_{rm}(k)) \quad (26)$$

and

$$M = \frac{P(1)}{b_1 P(z)} \quad (27)$$

$$N = \frac{a_1}{b_1} \quad (28)$$

$$R = \frac{1}{1 + \frac{\rho}{b_1^2} \left(\frac{Q(z)}{P(z)}\right)^2} \quad (29)$$

The predictive controller is shown in Figure 1. The block diagram of the predictive control includes a command gradation $M(z)$, a controller $R(z)$, a plant $P(z)$, and a feedback gain N . The structure is very similar to a standard control system; however, the parameters can be systematically derived. Unlike [16], this paper outlines a systematic closed-loop block diagram of the predictive controller, which provides a clear feedback control structure for an IPMSM drive system. This is an unprecedented method of predictive control and also a major aspect of this paper.

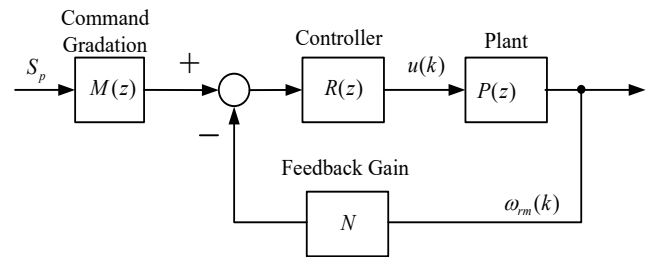


Figure 1 Block diagram of predictive speed-loop control.

2.3. Stability Analysis of the Proposed Drive System

The desired torque command of an IPMSM can be generated by the following equation

$$\frac{d}{dt} \omega_{rm}^* = \frac{1}{J_m} (T_e^* - T_L - B_m \omega_{rm}^*) \quad (30)$$

In the real world, there are parameter variations of the IPMSM and the external load measuring error. To compensate for that, the total equivalent load with uncertainty can be expressed as T_D , which includes the summation of the external load, the load influenced

by the parameter variations, torque tracking errors of both MTPA and flux weakening, and external load measuring error. Then (30) can be rewritten as

$$\frac{d}{dt}\omega_{rm}^* = \frac{-B_m}{J_m}\omega_{rm}^* + \frac{1}{J_m}T_e - T_D \quad (31)$$

and

$$T_D = \frac{1}{J_m}(\Delta J_m \frac{d}{dt}\omega_{rm}^* + \Delta B_m \omega_{rm}^* + T_L) \quad (32)$$

where T_D is the total load disturbance, ΔJ_m is the variation of inertia, and ΔB_m is the variation of the viscous coefficient. Next, the dynamic speed equation of the IPMSM is

$$\frac{d}{dt}\omega_{rm} = \frac{-B_m}{J_m}\omega_{rm} + \frac{1}{J_m}T_e - \hat{T}_D \quad (33)$$

Where \hat{T}_D is the estimated total load disturbance, which includes the influence of the motor parameters' uncertainty. The tuning step of the θ_{adv} , which is 0.18° , creates a varying torque that is less than 1% of the output torque T_e . As a result, the influence of the uncertainty is bound. The speed error, which is the difference between the speed command and the real speed, can be expressed as

$$e = \omega_{rm}^* - \omega_{rm} \quad (34)$$

Taking the differential of the speed error, one can obtain

$$\dot{e} = \frac{d}{dt}(\omega_{rm}^* - \omega_{rm}) = \frac{d}{dt}\omega_{rm}^* - \frac{d}{dt}\omega_{rm} \quad (35)$$

Substituting (31) and (33) into (35), one can obtain

$$\begin{aligned} \dot{e} &= \left(\frac{-B_m}{J_m}\omega_{rm}^* + \frac{1}{J_m}T_e - T_D\right) - \left(\frac{-B_m}{J_m}\omega_{rm} + \frac{1}{J_m}T_e - \hat{T}_D\right) \\ &= \frac{-B_m}{J_m}(\omega_{rm}^* - \omega_{rm}) - \tilde{T}_D \end{aligned} \quad (36)$$

We can define the load estimation error as $\tilde{T}_D = T_D - \hat{T}_D$. Assuming the external load changes slowly when compared to the quick responses of the speed control loop, it is possible to let $\dot{\tilde{T}}_D = 0$. The differential of the estimated load, therefore, can be expressed as follows

$$\dot{\tilde{T}}_D = -\hat{\tilde{T}}_D \quad (37)$$

Define a lyapunov function as

$$V = e^2 + \frac{1}{k_1}(\tilde{T}_D)^2 \quad (38)$$

where k_1 is a weighting factor. By taking the derivative of the Lyapunov function, one can derive

$$\dot{V} = 2e\dot{e} + \frac{2}{k_1}\tilde{T}_D\dot{\tilde{T}}_D \quad (39)$$

Substituting (36) into (39), one can obtain

$$\dot{V} = 2e\left(\frac{-B_m}{J_m}e - \tilde{T}_D\right) + \frac{2}{k_1}\tilde{T}_D\dot{\tilde{T}}_D = 2\frac{-B_m}{J_m}e^2 + 2\tilde{T}_D\left(\frac{1}{k_1}\dot{\tilde{T}}_D - e\right) \quad (40)$$

According to (40), it is possible to choose an adaption law as follows

$$\dot{\tilde{T}}_D = k_1 e \quad (41)$$

Substituting (41) into (40), we can obtain the differential of Lyapunov function as

$$\dot{V} = 2\frac{-B_m}{J_m}e^2 \leq 0 \quad (42)$$

From (42), the differential of Lyapunov function is negative semi-definite. Then, Barbalet lemma can be applied. First, a function y_1 is set, which is equal to \dot{V} . Next, by integrating the y_1 , we can obtain

$$\int_0^\infty y_1(\tau)d\tau = V(0) - V(\infty) < \infty \quad (43)$$

From (43), we can conclude

$$\lim_{t \rightarrow \infty} y_1(t) = 0 \quad (44)$$

According to (44), the speed error converges to zero as time approaches infinity.

3. MTPA Control and Flux-weakening Control

3.1. Basic Principle

The dynamic d-q axis voltages of an IPMSM can be expressed as

$$v_d = r_s i_d + L_d \frac{di_d}{dt} - \omega_{re} L_q i_q \quad (45)$$

and

$$v_q = r_s i_q + L_q \frac{di_q}{dt} - \omega_{re} L_d i_d + \omega_{re} \lambda_m \quad (46)$$

The total output torque of an IPMSM is

$$\begin{aligned} T_e &= \frac{3P}{2} [\lambda_m + (L_d - L_q) i_d] i_q \\ &= \frac{3P}{2} [\lambda_m i_q - (L_d - L_q) \sqrt{I_s^2 - i_q^2}] i_q \end{aligned} \quad (47)$$

Where I_s is the current amplitude. Two major control algorithms can be derived from (47) and can be used to adjust the torque of an IPMSM: field-oriented control and MTPA control. The field-oriented control sets a fixed d-axis current and adjusts the q-axis current to obtain linear proportional torque. The MTPA control sets a variable d-axis current, which is related to the q-axis current, to obtain maximum torque/ampere. The method can generate more torque than field-oriented control. However, the method creates a nonlinear relationship between the torque and q-axis current [3], which is a disadvantage of MTPA control. While it is a fact that MTPA's influence on torque linearity is a drawback, achieving maximum torque is a greater benefit that outweighs that disadvantage. The issue will be researched further by the authors of this paper.

Taking $\frac{d}{di_q} T_e = 0$ and substituting it into (47), we can obtain

$$\frac{3P}{2} [\lambda_m + (L_d - L_q) i_d - (L_d - L_q) i_q^2 \frac{1}{i_d}] = 0 \quad (48)$$

From (48), the d-axis current under MTPA control can be expressed as

$$i_d|_{MTPA} = \frac{-\lambda_m}{2(L_d - L_q)} - \sqrt{\frac{\lambda_m^2}{4(L_d - L_q)^2} + i_q^2} \quad (49)$$

The advance angle under MTPA control is

$$\theta_{MTPA} = \sin^{-1} \frac{i_d|_{MTPA}}{I_s} \quad (50)$$

and the current amplitude I_s is expressed as

$$I_s = \sqrt{i_d^2 + i_q^2} \quad (51)$$

In steady-state and neglecting the voltage drops of the resistance and inductance, it is not difficult to obtain

$$v_d = -\omega_{re} L_q i_q \quad (52)$$

and

$$v_q = \omega_{re} L_d i_d + \omega_{re} \lambda_m \quad (53)$$

The voltage amplitude is

$$v_s = \sqrt{(v_d^2 + v_q^2)} \quad (54)$$

If V_{om} is the maximum voltage amplitude, the voltage constraint can be shown as

$$(L_q i_q)^2 + (L_d i_d + \lambda_m)^2 = \left(\frac{V_{om}}{\omega_{re}}\right)^2 \quad (55)$$

The maximum current amplitude I_{sm} can be expressed as

$$i_d^2 + i_q^2 = I_{sm}^2 \quad (56)$$

From (56), it is easy to obtain

$$i_q = \sqrt{I_{sm}^2 - i_d^2} \quad (57)$$

Combining (49), (54), and (57), the constraints of the IPMSM drive system can be obtained. The drive system operates under MTPA control when the motor speed is below the rated base-speed. After the drive system reaches its base speed, there are two constraints: the current constraint of the maximum amplitude, I_{sm} , and the voltage constraint of the maximum voltage amplitude, V_{om} . However, the $\frac{V_{om}}{\omega_{re}}$ is decreased as the motor speed increases, which is shown in Figure 2. As a result, the axes of the ellipse are reduced when the motor speed increases. When $\omega_{re} < \omega_{base}$, the motor operates under MTPA control, which is indicated as OCBA in Figure 2. When $\omega_{base} < \omega_{re} < \omega_c$, the motor operates in region II, in which the motor can operate either under MTPA control or flux-weakening control. If $i_d < i_d|_{MTPA}$, MTPA control is used; on the other hand, if $i_d > i_d|_{MTPA}$, flux-weakening control is used. When $\omega_c < \omega_{re}$, the motor operates in region III, in which only flux-weakening control can be used.

3.2. Proposed Real-Time Flux-weakening Control

In the real world, flux-weakening control is very complicated because it requires λ_m, L_d , and L_q , which are very difficult to measure [15].

To solve this difficulty, in this paper, a real-time tuning flux-weakening control is proposed. First, the voltage amplitude of the IPMSM, v_s , which is expressed in (54) is compared to the maximum voltage amplitude, V_{om} . The θ_{FW} , which is shown in Figure 3(a), is tuned as follows

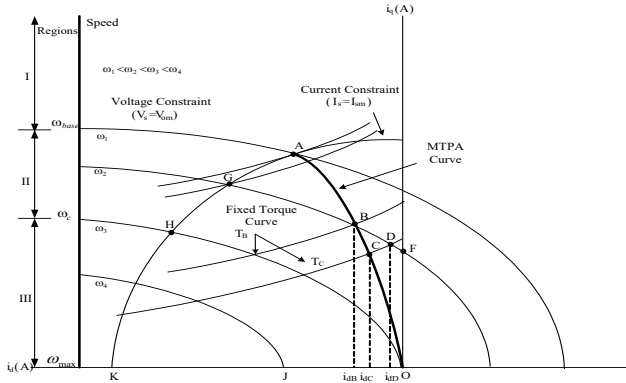


Figure 2 Operating regions of an IPMSM.

$$\theta_{FW}(k) = \theta_{FW}(k-1) + \alpha \cdot \text{sgn}(v_s - V_{om}) \quad (58)$$

and

$$\text{sgn}(v_s - V_{om}) = -1 \quad \text{when } (v_s - V_{om}) < 0 \quad (59a)$$

and

$$\text{sgn}(v_s - V_{om}) = 1 \quad \text{when } (v_s - V_{om}) \geq 0 \quad (59b)$$

where α is the step size of the real-time tuning control. By using (58), (59a), and (59b), the θ_{FW} can be real-time tuned, as shown in Figure 3(a)(b). Finally, a block diagram of the proposed real-time tuning flux-weakening control is shown in Figure 4. First, the amplitude of the desired output voltage v_s is calculated. Next, the desired output voltage, v_s , is compared with the measured output voltage, V_{om} . After that, (58) is used to compute the $\theta_{FW}(k)$. Similar to previous research [2]-[5], [21], the proposed flux-weakening control method reduces the torque at high-speed operating range, and is not guaranteed the torque linearity. This is a common characteristic of flux-weakening control algorithms. However, the stability analysis of the whole drive system is discussed in the previous section of this paper.

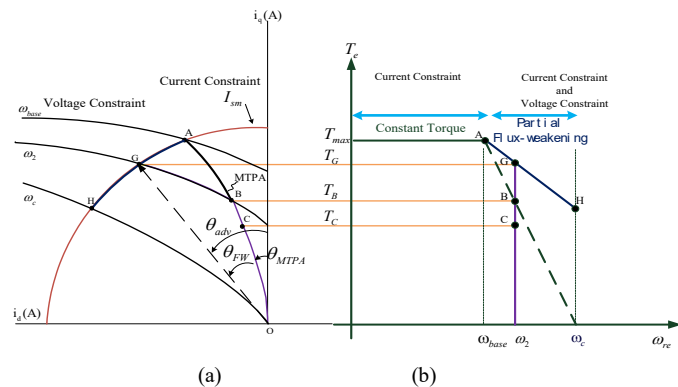


Figure 3 Operating curves and torque-speed curves of an IPMSM (a) operating curves (b) torque-speed curves.

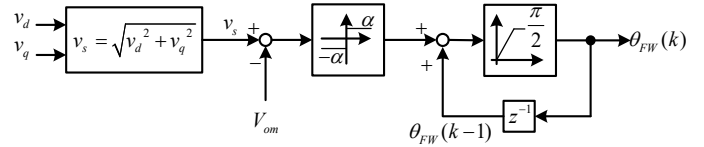


Figure 4 Block diagram of the proposed flux-weakening control.

4. Implementation

The implemented IPMSM drive system is shown in Figure 5(a) and (b). Figure 5(a) is a block diagram of the proposed IPMSM. The system consists of two main parts: the DSP system and the hardware circuit. The DSP system uses a TMS-320F-28335, which is a 32-bit, digital signal processor manufactured by Texas Instruments. The sampling interval of the current-loop control is 100 μ s, while that of the speed-loop control is 1 ms.

Taking the MTPA operating region as an example, the controller works as follows. First, as shown in Figure 5(a) and based on the predictive speed controller, after the speed command is input and the motor speed is feedback, the q-axis current i_{qp} is computed. Second, the load compensator compensates for the load disturbance \hat{T}_D and then generates the compensation current i_{qT_D} . Then the total q-axis current command, which is the summation of the i_{qp} and i_{qT_D} , is computed and expressed as i_q^* .

Next, the d-axis current is computed through (49) when the motor is operating in the MTPA region. After that, the advance phase angle θ_{MTPA} and stator current amplitude I_s^* are computed by using (50) and (51). Finally, the flux-weakening is obtained by adding θ_{FW} .

By using the MTPA table and the real-time tuning flux-weakening control, the advance angle of the current can be obtained. After that, the d-axis current command i_d^* and the q-axis current command i_q^* are calculated. A current regulated control and a space vector PWM modulation are executed. Finally, the switching states of the inverter are determined and output. A closed-loop system can thus be obtained. A DC motor is coupled with the IPMSM. The motor parameters are: $L_q = 31 \text{ mH}$, $L_d = 15 \text{ mH}$, $\lambda_m = 0.227 \text{ v.sec/rad}$, and $R_s = 1.9 \Omega$. The motor is 4-pole, 1-HP, and rated at 1500 r/min.

Figure 5(b) shows a photograph of the entire hardware circuit, which includes a DSP, gate drivers, peripheral devices, current sensing circuits, and an inverter. Figure 5(c) shows a photograph of the implemented IPMSM drive system, including an IPMSM and a dynamometer.

5. Experimental Results

The performance of the proposed flux-weakening control for an IPMSM drive system was evaluated according to experimental results. Figure 6(a) shows the measured steady-state torque-speed curves using the zero d-axis current control and the MTPA control. Figure 6(b) shows measured steady-state torque-speed curves

using the MTPA control and the hybrid control, which is a combination of the MTPA control and the flux-weakening control.

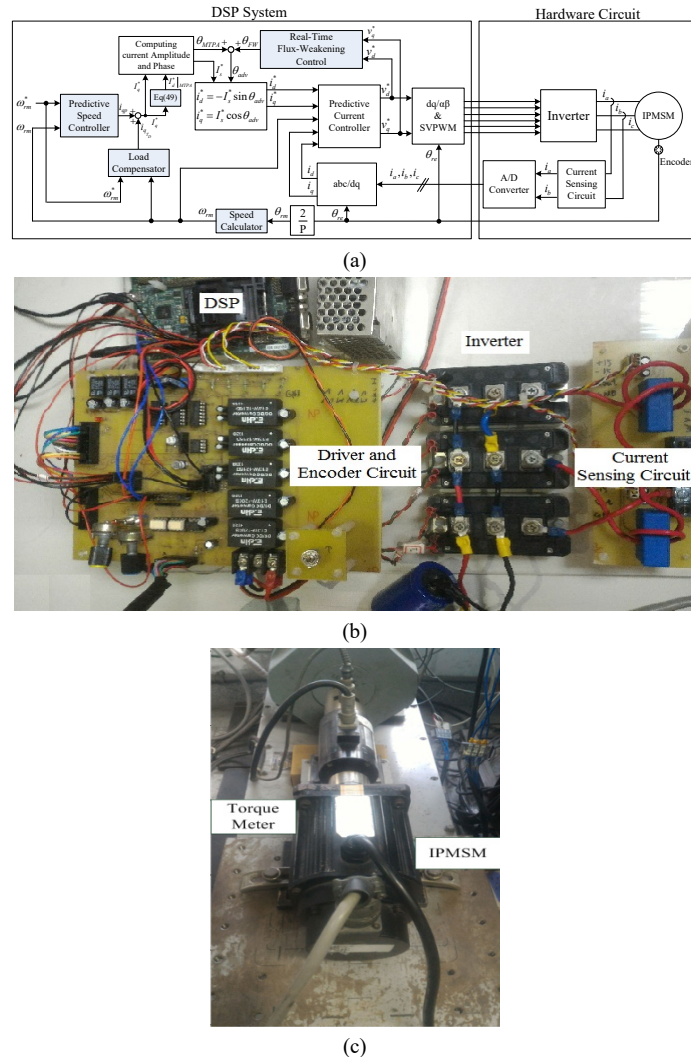


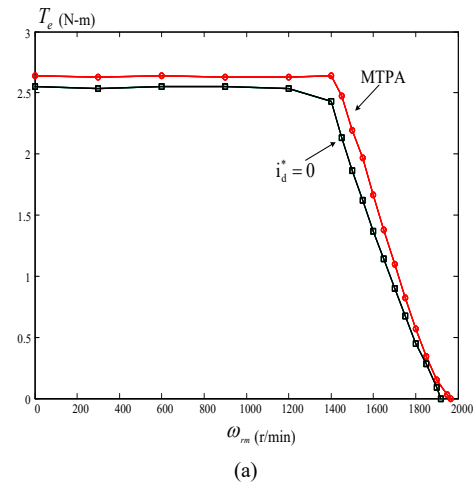
Figure 5 The implemented IPMSM drive system
(a) block diagram (b) hardware circuit (c) motor and dynamometer.

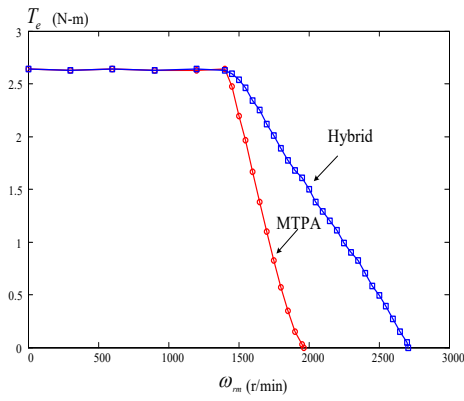
As you can observe, the hybrid control has better performance than the MTPA control. Figure 6 (c) shows the q-axis current to the d-axis current trajectory when the IPMSM is operating from the MTPA control region to the flux-weakening control region. The d-axis current increases slightly in the MTPA region; however, the d-axis current increases significantly in the flux-weakening region.

Figure 7(a)(b) and (c) show the measured waveforms of the IPMSM operating at 1800 r/min under loads of 0.57 N-m and 1.89 N-m. Figure 7(a) is the amplitude of the stator current I_s . Figure 7(b) shows the relative measured d-axis and q-axis currents. Figure 7(c) shows the measured advance angle θ_{adv} that is the sum of the θ_{FW} and θ_{MTPA} , which are the measured flux-weakening angle and the measured MTPA control angle. The delay of the measured responses is due to the lag between the load command and the external load that is generated by the dynamometer. Figure 8(a) shows the load disturbance responses when using the proposed predictive controller, the previous predictive controller that was proposed by [21], and the PI controller. The parameters of the PI

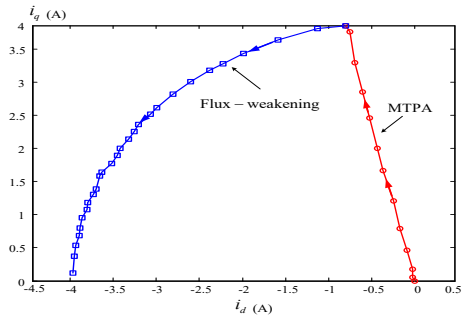
controller are obtained by using the pole assignment technique. The locations of the desired poles for the closed-loop drive system are assigned as $-4.06+j0.13$ and $-4.06-j0.13$, respectively. The proposed predictive controller performs better than the previous predictive controller and the PI controller. At this 2000 r/min high speed, the field weakening algorithm is applied. The maximum allowed external load at this operating speed is 1.6 N.m. Experimental results show the proposed predictive controller performs the best. Figure 8(b) shows the repetitive 1.6 N.m load disturbance responses. The proposed predictive controller performs well again.

Figure 9(a) shows the measured step-input transient speed responses at the maximum speed, 2700 r/min. In this paper, the rated speed is 1500 r/min. The measured responses show the proposed predictive controller has a quicker rise time than the previous predictive controller proposed by [16] and the PI controller. Figure 9(b) shows the measured step-input transient speed responses at 3 r/min, which is the minimum operating speed. According to Figure 9(a) and Figure 9(b), we can conclude that the adjustable speed ratio of the maximum speed to minimum speed is 900:1. Figure 10 (a)(b)(c)(d) shows the current command and measured current errors using different controllers. Again, the proposed predictive controller has the smallest tracking errors. Figure 11(a)(b)(c) show the measured dynamic responses of the proposed flux-weakening control at 1800 r/min. A 5V step input at V_{om} is injected for every 1 second. The real voltage amplitude of the motor, which is expressed as v_s can track the voltage command V_{om} well. The rise time of the voltage control is about 50 ms. Figure 11(a), Figure 11(b) and Figure 11(c) show the responses of speed, voltage amplitude, and controlling angle θ_{FW} respectively. Figure 12(a) shows the measured efficiency of the whole drive system. The proposed method has higher efficiency than the linear flux-weakening method that was proposed by [21]. The major reason is that the proposed method provides greater output torque at the same motor speed. Figure 12(b) and (c) show the measured speed responses as the inertia of the drive system is increased to 5 times. The proposed predictive controller can provide a lower overshoot and a shorter settling time as the inertia increases.



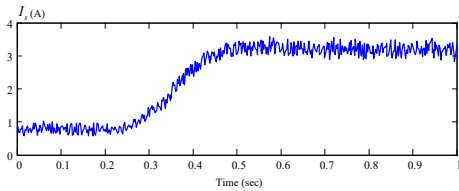


(b)

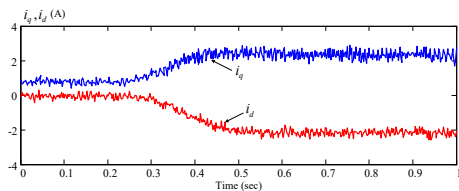


(c)

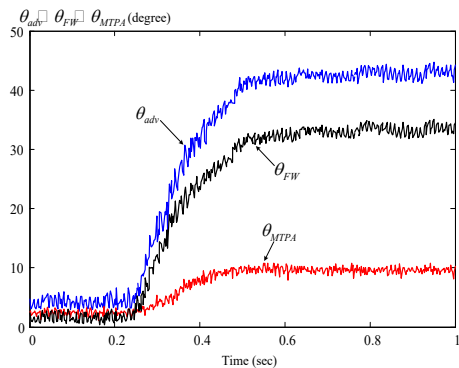
Figure 6 Measured steady-state characteristic curves
(a)MTPA and zero d-axis current (b) MTPA and hybrid control
(c) q-axis current to d-axis current curve.



(a)

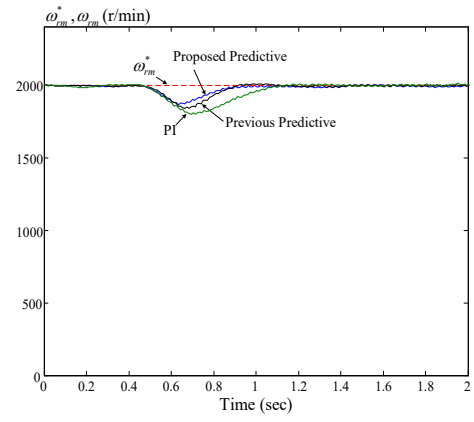


(b)

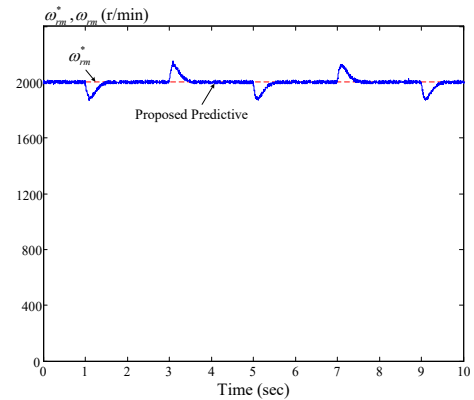


(c)

Figure 7 Measured 1800 r/min with loads of 0.57 N-m and 1.89 N-m
(a) I_s (b) measured d-q axis currents (c) advance angle.

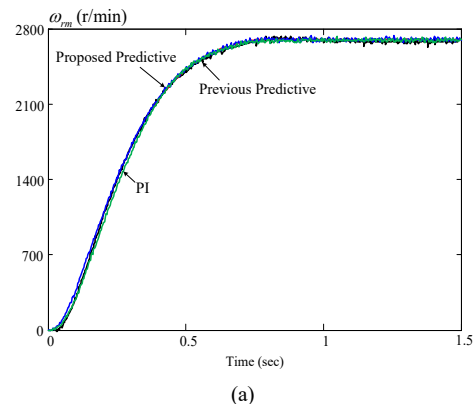


(a)

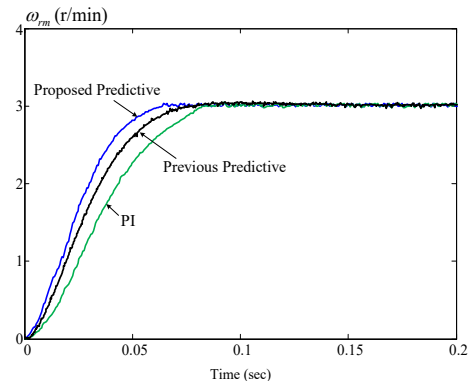


(b)

Figure 8 Measured field weakening operating speed with a large 1.6 N.m external load.
(a) step-input load (b) repetitive loads.



(a)



(b)

Figure 9 Measured step-input transient speed responses
(a) highest speed (b) lowest speed.

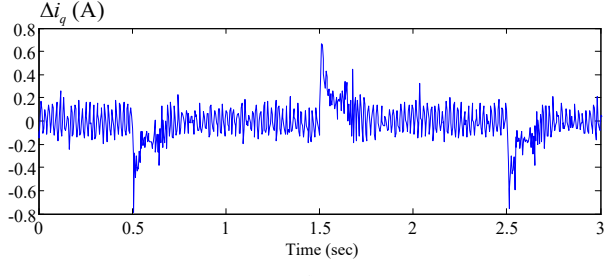
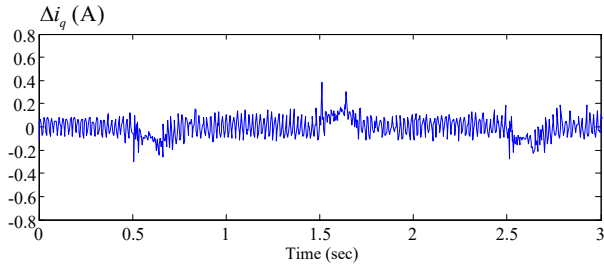
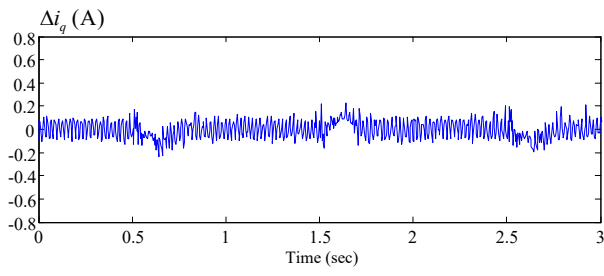
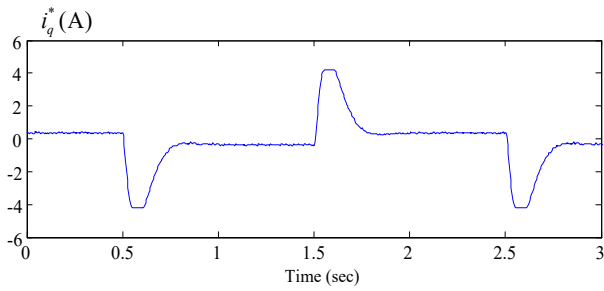


Figure 10 Comparison of measured current responses using different controllers (a) current command (b) proposed predictive (c) previous predictive (d) PI.

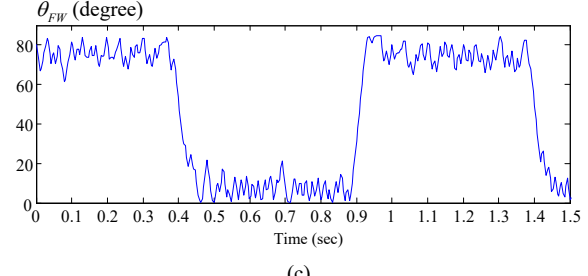
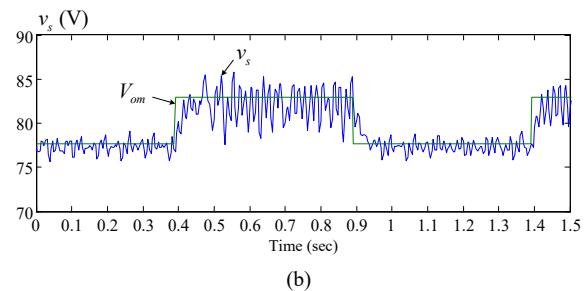
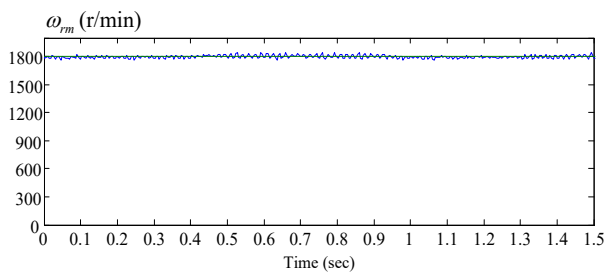
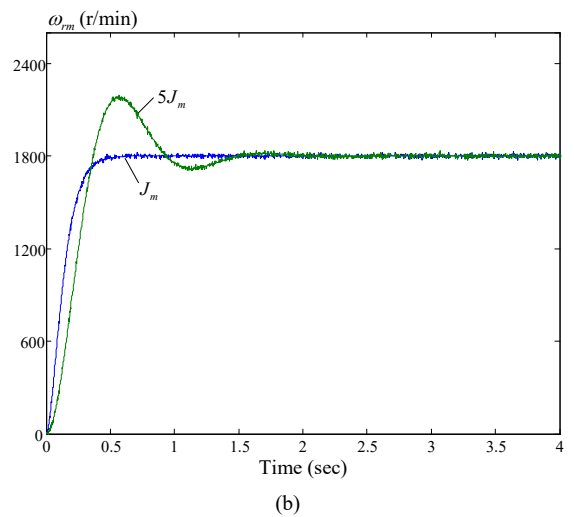
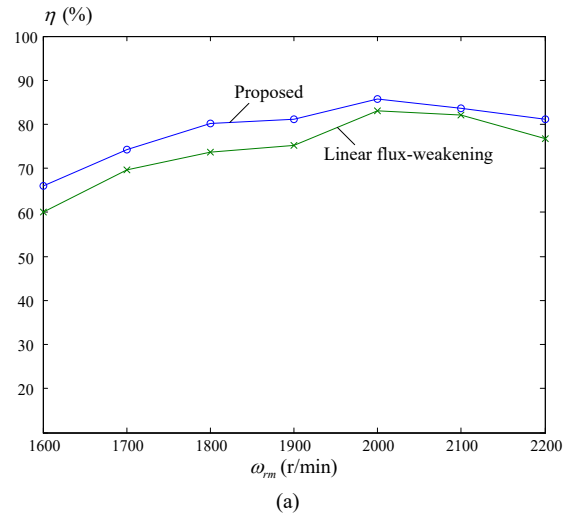
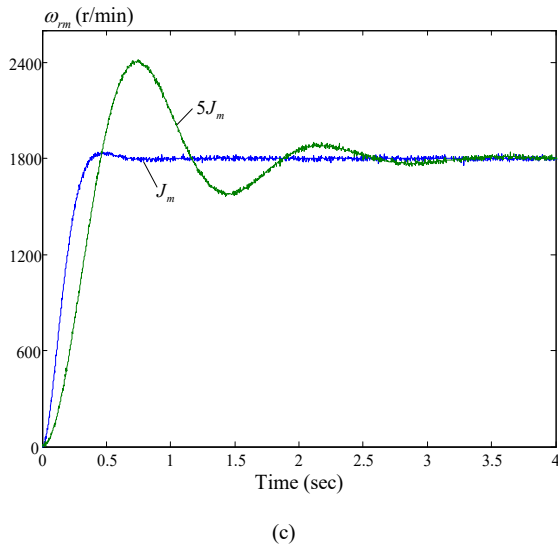


Figure 11 Measured dynamic responses of the flux-weakening control at 1800 r/min

(a) speed (b) voltage magnitude regulation (c) θ_{FW} .





(c)
Figure 12 Measured efficiency and varied inertia speed responses. (a) efficiency (b) proposed predictive controller (c) PI controller.

6. Conclusions

In this paper, an MTPA control and a real-time flux-weakening control drive system using a predictive controller is proposed to improve the adjustable speed range and dynamic responses of an IPMSM. Experimental results show that the proposed drive system has good performance, including fast transient responses, good load disturbance rejection capability, and good tracking responses. Furthermore, the proposed method is easily implemented by using a DSP. Experimental results validate the theoretical analysis.

References

- [1] T. H. Liu, S. K. Tseng, and M. B. Lu, "Auto-tuning flux-weakening control for an IPMSM drive system using a predictive controller," IEEE 26th International Symposium on Industrial Electronics (ISIE), 238-243, 2017.
- [2] S. Bolognani, S. Calligaro, and R. Petrella, "Adaptive flux-weakening controller for interior permanent magnet synchronous motor drives," IEEE J. of Emerg. and Sel. Top. in Pow. Electron., 2(2), 236-248, June 2014.
- [3] H. Liu, Z. Q. Zhu, E. Mohamed, Y. Fu, and X. Qi, "Flux-weakening control of nonsalient pole PMSM having large winding inductance, accounting for resistive voltage drop and inverter nonlinearities," IEEE Trans. on Pow. Electron., 27(2), 942-952, Feb. 2012.
- [4] T. S. Kwon, G. Y. Choi, M. S. Kwak, and S. K. Sul, "Novel flux-weakening control of an IPMSM for quasi-six-step operation," IEEE Trans. on Ind. Appl., 44(6), 1722-1731, Nov./Dec. 2008.
- [5] C. T. Pan and J. H. Liaw, "A robust field-weakening control strategy for surface-mounted permanent-magnet motor drives," IEEE Trans. on Energy Convers., 20(4), 701-709, Dec. 2005.
- [6] M. N. Uddin and M. M. I. Chy, "Online parameter-estimation-based speed control of PM AC motor drive in flux-weakening region," IEEE Trans. on Ind. Appl., 44(5), 1486-1494, Sep./Oct. 2008.
- [7] S. M. Sue and C. T. Pan, "Voltage-constraint-tracking-based field-weakening control of IPM synchronous motor drives," IEEE Trans. on Ind. Electron., 55(1), 340-347, Jan. 2008.
- [8] S. Y. Jung, C. C. Mi, and K. Nam, "Torque control of IPMSM in the field-weakening region with improved DC-link voltage utilization," IEEE Trans. on Ind. Electron., 62(6), 3380-3387, June 2015.
- [9] S. Chatithongsuk, B. Nahid-Mobarakeh, J. P. Caron, N. Takorabet, and F. Meibody-Tabar, "Optimal design of permanent magnet motors to improve

field-weakening performances in variable speed drives," IEEE Trans. on Ind. Electron., 59(6), 2484-2494, June 2012.

- [10] K. C. Kim, "A novel magnetic flux weakening method of permanent magnet synchronous motor for electric vehicles," IEEE Trans. on Magn., 48(11), 4042-4045, Nov. 2012.
- [11] V. R. Jevremovic and D. P. Marcetic, "Closed-loop flux-weakening for permanent magnet synchronous motors," Conference on Power Electronics, Machines and Drives, PEMD 2008, 4th IET, 717-721, Apr. 2008.
- [12] L. Harnefors, K. Pietilainen and L. Gertmar, "Torque-maximizing field-weakening control: design, analysis, and parameter selection," IEEE Trans. on Ind. Electron., 48(1), 161-168, Feb. 2001.
- [13] O. Wallmark, "On control of permanent-magnet synchronous motors in hybrid-electric vehicle applications," Technical Reports at the School of Electric Engineering, Technical Report, no. 495L, Chalmers University of Technology, Master Thesis, 2004
- [14] N. Bedetti, S. Calligaro and R. Petrella, "Analytical design of flux-weakening voltage regulation loop in IPMSM drives," IEEE Energy Conversion Congress and Exposition (ECCE), ECCE 2015, 6145-6152, Sep. 2015.
- [15] M. Pacas and J. Weber, "Predictive direct torque control for the PM synchronous machine," IEEE Trans. on Ind. Electron., 52(5), 1350-1356, Sep. 2005.
- [16] S. Bolognani, S. Bolognani, L. Peretti, and M. Zigliotto, "Design and implementation of model predictive control for electrical motor drives," IEEE Trans. on Ind. Electron., 56(6), 1925-1936, June 2009.
- [17] J. M. Kim and S. K. Sul, "Speed control of interior permanent magnet synchronous motor drive for the flux weakening operation," IEEE Trans. on Ind. Appl., 33(1), 43-48, Jan./Feb. 1997.
- [18] E. J. Fuentes and C. A. Silva, "Predictive speed control of a two-mass system driven by a permanent magnet synchronous motor," IEEE Trans. on Ind. Electron., 59(7), 2840-2848, July 2012.
- [19] M. Siami, D. A. Khaburi, A. Abbaszadeh, and J. Rodriguez, "Robustness improvement of predictive current control using prediction error correction for permanent-magnet synchronous machines," IEEE Trans. on Ind. Electron., 63(6), 3458-3466, June 2016.
- [20] T. Tarczewski and L. M. Grzesiak, "Constrained state feedback speed control of PMSM based on model predictive approach," IEEE Trans. on Ind. Electron., 63(6), 3867-3875, June 2016.
- [21] K. Chen, Y. Sun, and B. Liu, "Interior permanent magnet synchronous motor linear field-weakening control," IEEE Trans. on Energy Convers., 31(1), 159-164, Mar. 2016.